Stator/Rotor Interaction in a Transonic Turbine

Michael B. Giles*
Massachusetts Institute of Technology, Cambridge, Massachusetts 02139

This paper presents calculations of a stator/rotor interaction in a highly loaded transonic first turbine stage. Of particular interest is the propagation and reflection of shocks which originate at the trailing edge of the upstream stator. These produce a 40% variation in the lift on the rotor, which would cause structural vibrations and increased losses. Also, the unsteady shocks would cause temporary boundary-layer separation near the leading edge of the suction surface. The numerical procedure solves the inviscid unsteady Euler equations, including quasi-three-dimensional terms. The use of a conservative treatment guarantees the correct treatment of the moving shocks. A simple technique is used to couple the calculations on the stator and rotor grids. A key feature of the paper is the use of "time-inclined" computational planes to allow the analysis of cases in which the ratio of stator and rotor pitches is not equal to unity or the ratio of two small integers.

Introduction

In the last few years, an increasing amount of attention has been devoted to the calculation of unsteady flow in turbomachinery. Hodson[1] and Giles[2] have performed calculations of wake/rotor interaction in which incoming wakes were specified at inflow boundaries, and the resulting interaction was modeled using the inviscid Euler equations. Koya and Kotake,[3] Fourmaux,[4] and Lewis et al.[5] have calculated inviscid stator/rotor interactions in three dimensions, two dimensions, and quasi-three dimensions respectively. Finally, Rai has performed Navier-Stokes calculations of stator-rotor interaction in two dimensions[6] and three dimensions.[7]

The purpose of this paper is to add to this previous body of research in three areas. The first is an extremely simple method for handling the unsteady stator/rotor interface using two separate stator and rotor grids with a gap, which is bridged by a set of shearing computational cells. The treatment is fully conservative and therefore is suitable for applications in which shocks pass across the interface.

The second area of interest is the use of time-inclined computational planes to treat the difficulties encountered when the stator/rotor pitch ratio is not a small integer ratio, which is what has been assumed by most researchers. Hodson[1] and Koya[3] used a technique due to Erdos,[8] which involves a large amount of computer storage and a critical assumption that the flow is temporally periodic as well as spatially periodic. In Ref. 2 it was explained why this assumption is invalid for viscous flows, and an alternative approach was introduced. This involves "inclining" the computational plane such that different nodes at a given time-level are actually at different physical times. This technique was used for wake/rotor calculations, and in this paper it is shown that the technique can be extended to stator/rotor calculations.

The final part of this paper presents an application to a stator/rotor interaction in a highly loaded transonic first turbine stage. An interesting feature in this highly unsteady flow is the oblique shock wave, which extends from the trailing edge of the stator. This shock impinges on the rotor blade, reflects upstream, and then reflects again off the stator blade suction surface. The calculation clearly captures the complicated shock motion and shows the large unsteadiness in the lift on the rotor blade.

Basic Numerical Method

The flowfield is modeled by the unsteady Euler equations. These are inviscid equations that in a conservative formulation correctly model the formation and motion of shocks as well as the entropy and vorticity generated by the shocks.

$$h\frac{\partial U}{\partial t}+\frac{\partial (hF)}{\partial x}+\frac{\partial (hG)}{\partial y}=S \tag{1}$$

where U, F, G and, S are four component vectors given by

$$U=\begin{bmatrix}\rho\\ \rho u\\ \rho v\\ \rho E\end{bmatrix} \tag{2}$$

$$F=\begin{bmatrix}\rho u\\ \rho u^2+p\\ \rho uv\\ \rho uH\end{bmatrix} \tag{3}$$

$$G=\begin{bmatrix}\rho v\\ \rho uv\\ \rho v^2+p\\ \rho vH\end{bmatrix} \tag{4}$$

$$S=\begin{bmatrix}0\\ p\dfrac{\partial h}{\partial x}\\ p\dfrac{\partial h}{\partial y}\\ 0\end{bmatrix} \tag{5}$$

Although these are two-dimensional equations, they include three-dimensional effects through the specification of the streamtube thickness h in the third dimension, which produces the source term on the right side of the equation. The pressure

Presented as Paper 88-3093 at the AIAA/SAE/ASME/ASEE 24th Joint Propulsion Conference, Boston, MA, July 11-13, 1988; received July 22, 1988; revision received July 28, 1989. Copyright © 1988 by the American Institute of Aeronautics and Astronautics, Inc. All rights reserved.

*Harold R. Edgerton Assistant Professor, Department of Aeronautics and Astronautics. Member AIAA.

p and total enthalpy H are related to the density ρ, velocity components u and v, and total energy per unit mass E by the following two equations which assume a perfect gas with a constant specific heat ratio γ.

$$p = (\gamma - 1)\rho\left[E - \tfrac{1}{2}(u^2 + v^2)\right] \tag{6}$$

$$H = E + p/\rho \tag{7}$$

These equations are also valid in the rotor frame of reference using rotor-relative velocities and total energy.

The numerical algorithm which is used is based upon Ni's formulation of the Lax-Wendroff algorithm.[9] It is a robust explicit method using an unstructured grid composed of quadrilateral cells. The flow variables are located at the vertices of the cells, and the flux across each cell face is based upon the average of the fluxes F and G at the corner nodes. Summing the fluxes through the four faces and adding the source term for the cell gives the flux residual. From this the changes in the flow variables are distributed back to the four corner nodes using the Lax-Wendroff algorithm, which guarantees numerical stability, subject to a time-step limit. To prevent non-physical oscillations, a numerical smoothing is used. It is a combination of a fourth difference smoothing in smooth flow regions plus an artificial bulk viscosity in the neighborhood of shocks. Since the scheme is a conservative approximation to the integral form of the unsteady Euler equations, both stationary and moving shocks are captured correctly, which is important for the application discussed later in this paper. Further details on the algorithm are available in Ref. 10.

Stator-Rotor Interface

The basic geometric approach for a case in which the stator and rotor pitches are equal is depicted in Fig. 1. The computational grid is composed of two parts, one part fixed to the stator blade rows, (which in this discussion will be assumed to be the upstream blade row) and the other part moving with the rotor blade row with velocity V. The two parts are separated by a cell width at the interface with equal grid node spacing along the interface on either side. To span the gap between the two halves, a set of quadrilateral cells are defined by connecting each stator grid node to the nearest rotor grid node. As time progresses, the rotor moves and the cells change from state 1 (with solid lines) to state 2 (with dotted lines) to state 3 (with dashed lines). At that time, the connecting lines are redefined to maintain nearest neighbor connections, and the cells revert to state 1.

As shown in Fig. 2, spatial periodicity is used to extend the rotor grid as needed as the rotor grid moves. The solid lines denote the actual position of the rotor grid, and the dotted lines show the position of the rotor grid shifted by one pitch. The open and closed circles denote pairs of rotor nodes, which are defined to be the same through the assumption of spatial periodicity.

On each half of the grid, the flow solution is calculated using local grid-relative flow variables. At the interface cells, the basic algorithm has to be modified. First, all flow variables are converted into the stator frame of reference. Second, the basic Lax-Wendroff algorithm must be modified due to the shearing of the computational cell. The change is best understood by considering the following integral form of the two-dimensional Euler equations on a control volume whose boundary has a unit normal vector n and is moving with velocity $V = (V_x, V_y)^T$.

$$\frac{\mathrm{d}}{\mathrm{d}t}\iint U\,\mathrm{d}x\,\mathrm{d}y = \iint \frac{\partial U}{\partial t}\,\mathrm{d}x\,\mathrm{d}y + \oint U(V.n)\mathrm{d}s$$

$$= -\oint (F - UV_x)\mathrm{d}y - (G - UV_y)\mathrm{d}x \tag{8}$$

Considering the computational cell A illustrated in Fig. 2, the extra flux term across face 1-2 is approximated by treating U as being linear.

$$\int_{x1}^{x2} UV_y\,\mathrm{d}x = \Delta x_{21}\int_0^1 \left[U_1 + \xi(U_2 - U_1)\right]\xi V\,\mathrm{d}\xi$$

$$= \Delta x_{21}\left(\tfrac{1}{6}U_1 + \tfrac{1}{3}U_2\right)V \tag{9}$$

This produces only a minor change to the flux evaluation in the Lax-Wendroff algorithm. A final modification is that the changes in the flow variables, which are distributed from the cell to the nodes on the rotor face, must be converted back into changes in rotor-relative variables. Complete details are available in Ref. 10.

Time-Inclined Computational Plane

When the number of stators and rotors is not equal, the flow does not have a simple spatial periodicity in the circumferential direction. This greatly complicates the periodic boundary condition.

Figure 3 shows, at two instants in time, a stator/rotor interaction in which the stator pitch is greater than the rotor pitch. At the first instant in time, the lower rotor is aligned with the lower stator. At the later time, the upper rotor is aligned with the upper stator. The time lag between the two instants is equal to the difference in pitches divided by the rotor wheel speed.

$$\Delta T = (P_s - P_r)/V \tag{10}$$

Using this time lag, one can now state that the flow on the lower periodic surface, which is one boundary of the computational domain, is equal to the flow on the upper surface at the later time. Thus the lagged periodic boundary condition is

$$U(x,y,t) = U(x,y + P_s, t + \Delta T) \tag{11}$$

in the stator frame of reference and

$$U(x,y,t) = U(x,y + P_r, t + \Delta T) \tag{12}$$

in the rotor frame of reference. The P_s and P_r are the stator and rotor pitches, respectively.

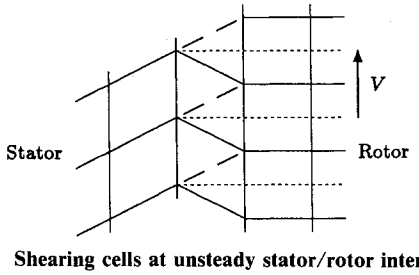

Fig. 1 Shearing cells at unsteady stator/rotor interface.

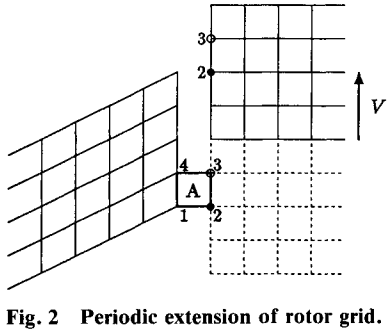

Fig. 2 Periodic extension of rotor grid.

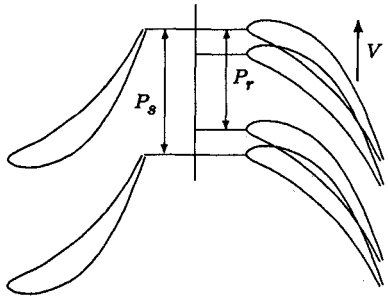

Fig. 3 Origin of lagged periodic boundary conditions.

Having discussed the mathematical formulation of the problem, the difficulty now is determining how to calculate the flow numerically and implement the periodic boundary condition. If the pitch ratio P_s/P_r is unity, then one simply enforces periodicity by letting the computational grid "wrap round" so that the points on the periodic line are treated exactly the same as any other points in the grid.

Erdos[8] was the first to develop a method of treating unequal pitches. As illustrated in Fig. 4, his procedure involves setting values at dummy points along each periodic line from stored values at points along the other periodic line at earlier times. Mathematically this corresponds to using the equations

$$U(x,y,t) = U(x,y-P_s,t-\Delta T) \tag{13a}$$

$$U(x,y,t) = U(x,y-P_r,t-\Delta T) \tag{13b}$$

for points on the upper periodic line segments in the stator and rotor grids and

$$U(x,y,t) = U[x,y+P_s,t-(T-\Delta T)] \tag{14a}$$

$$U(x,y,t) = U[x,y+P_r,t-(T-\Delta T)] \tag{14b}$$

for points on the lower periodic line.

The implementation of this method requires storing the full solution along the periodic lines for a whole blade-passing period $T=P/V$. In addition, an unfortunate consequence is that by combining the above two equations, one can see that this forces the numerical solution on the periodic lines to be periodic in time with period T. This is probably valid only when calculating inviscid flows. In viscous flows, there are physical instabilities and oscillations, such as vortex shedding at the trailing edge, in which the frequency is not a multiple of the blade-passing frequency. In these situations, Erdos' method would fail to converge to a consistent periodic solution.

An alternative solution to this problem was presented in Ref. 2. If, as illustrated in Fig. 5, one inclines the computational grid in time by an amount $\Delta T/P$ then one automatically satisfies the lagged periodic boundary condition by simply wrapping round on the computational grid as before. This avoids the assumption of temporal periodicity and completely eliminates the complexity of the Erdos approach at the expense of introducing complexity into the solution of the interior flow.

The effect of the inclined computational plane on the equations of motion can be found by considering the coordinate transformation from (x,y,t), the physical coordinates, to (x',y',t'), the computational coordinates in which t' is constant on each computational time level. The equations defining the transformation are

$$x' = x \tag{15a}$$

$$y' = y \tag{15b}$$

$$t' = t - \lambda y \tag{15c}$$

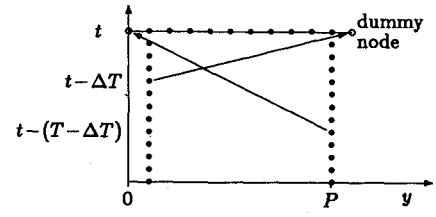

Fig. 4 Erdos' periodic boundary treatment.

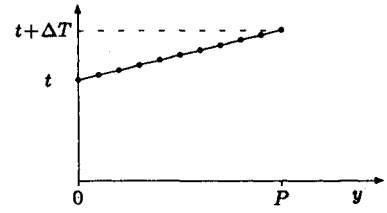

Fig. 5 Inclined computational plane.

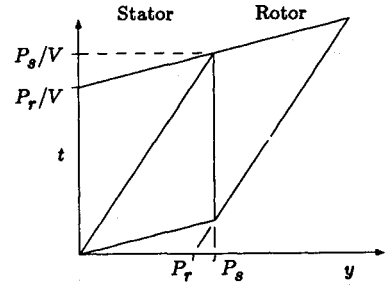

Fig. 6 Computational boundaries at interface.

and the inverse transformation is

$$x = x' \tag{16a}$$

$$y = y' \tag{16b}$$

$$t = t' + \lambda y' \tag{16c}$$

where

$$\lambda = \frac{\Delta T}{P} \tag{17}$$

When one transforms the Euler equations into the new computational coordinate system, the resultant equations are

$$h\frac{\partial}{\partial t'}\left(U-\lambda G\right)+\frac{\partial(hF)}{\partial x'}+\frac{\partial(hG)}{\partial y'}=S \tag{18}$$

Thus the conservation state variables have changed from U to $Q=U-\lambda G$. This change in the conservation variables requires just minor changes to the basic numerical algorithm because fortunately one can calculate U from Q in closed form for a perfect gas. Full details are given in Refs. 10 and 11.

In stator/rotor calculations, the stator and rotor grids require different values of λ, since ΔT is the same for both, and the pitches are different. In addition, the time steps are different on the two grids because the blade passing period is different in the two frames of reference, and the calculation requires matching numbers of timesteps per period. At the interface between the two grids, the same basic approach is used with shearing cells on the inclined computational plane in the stator frame of reference. It becomes much harder, however, to visualize the computational cell, and the details of the numerical algorithm become much more complex.[10]

To explain some of the features of the inclined planes at the interface, Fig. 6 shows the boundaries, in the y-t plane, of the

stator and rotor grids at the interface over one blade-passing period. Note how the rotor pitch is less than the stator pitch but appears to be equal to it on the inclined computational plane. This is what produces the simple spatial periodicity on the inclined plane and suggests that this may be a useful viewpoint for performing data reduction in experiments. Note also that the rotor period is larger than the stator period, but the beginning of both periods and the end of both periods appear on the same inclined plane.

Results

This section shows results obtained for a highly loaded transonic first turbine stage which has been tested at both Massachusetts Institute of Technology[12] and Oxford University.[13,14] Before examining the unsteady behavior due to the stator/rotor interaction, it is helpful to first examine results obtained with a steady-state calculation. In this calculation, the average stator outflow conditions are matched to the average rotor inflow conditions, and the rotor wheel speed has been adjusted to achieve the correct rotor-relative inflow angle. Steady-state nonreflecting boundary conditions are used so that outgoing shocks are not artificially reflected at the outflow boundaries.[15] This would be a problem if one used the standard boundary conditions that impose uniform pressure across the outflow.

Figure 7 shows the overall geometry of the stage as well as pressure contours for the coupled steady stator/rotor calculation. The pitch ratio is approximately 1.69, which causes difficulties for the subsequent unsteady calculation. If one uses a computational grid with one stator and one rotor, then the value of λ which is required exceeds certain domain-of-dependence limitations which are described in Ref. 11. Instead, the calculation is performed with one stator and two rotors. This gives an effective pitch ratio of $1.69/2 = 0.85$, which in turn gives a value of λ which is acceptable.

The computation was performed on a three-processor Alliant FX/8, which is approximately 20 times faster than a Microvax II. The computational grid contains a total of 18,000 cells. The steady calculation took 4 h to converge to a steady state, and the unsteady calculation took 8 h to calculate 8 periods using 1400 iterations per period. Eight periods were sufficient to obtain a converged periodic solution.

Table 1 lists the flow conditions used in the steady-flow calculation. The value of γ, the ratio of specific heats, is typical of air and combustion products leaving the combustor. The rotor Mach number was chosen to achieve the correct rotor-relative inflow angle. The outflows of both the stator and rotor are supersonic producing weak oblique shocks at the trailing edges, which can be seen in Fig. 7. In the case of the stator, the oblique shock, which is incident on the suction surface, produces a noticeable reflection. In this calculation the stream-tube height h decreases linearly by 14% through the stator and then increases linearly by 22% through the rotor and is constant upstream, downstream, and between the blade rows. These values were obtained from a streamline curvature analysis which included the effect of injected cooling flow.

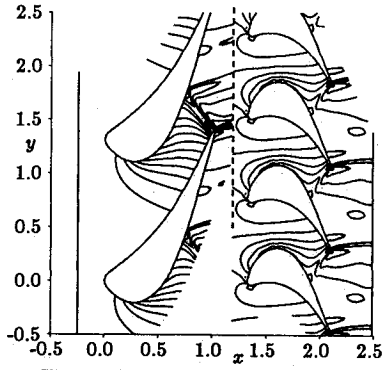

Fig. 7 Steady pressure contours.

The decrease in the streamtube height through the stator decreases the inflow Mach number by increasing the ratio of the inflow area to the throat area. Similarly, the large increase in the stream-tube thickness through the rotor produces the large rotor-relative inflow Mach number and the high Mach numbers along the leading portion of the suction surface.

Figures 8 and 9 show the surface pressure and Mach number distributions on both blades. The rapid drop in pressure and rise in Mach number on the suction surfaces, ahead of the impinging oblique shock wave, is due to the supersonic expansion wave, which leaves the trailing edge just ahead of the oblique shock. The sharp pressure rise at the trailing edges is due to the use of a cusp to close the finite thickness trailing edge. The surface pressures on the rotor are generally lower than on the stator because the rotor-relative stagnation pressure is a factor 0.58 smaller than the inlet stagnation pressure (which is used as the nondimensionalizing reference value). Finally, note that almost the entire rotor suction surface is supersonic due to the high inflow Mach number. This leads to dramatic unsteady flow effects.

Figure 10 shows pressure contours for the unsteady stator/rotor interaction at eight intervals during one stator period. To aid the discussion of these results, each pressure contour plot is accompanied by a corresponding figure, which sketches the location and direction of motion of the shocks. These contour plots are on physical time levels defined by $t = \text{const}$, whereas the inclined computational time levels are defined by $t' = \text{const}$. Thus, to obtain these plots one has to interpolate between computational time levels. This is done by performing the flow calculation until the flow is periodic and then storing fifty flow solutions equally spaced through the period. Using Fourier modes, one can then reconstruct the flow at any instant in time. This postprocessing technique keeps storage requirements to a minimum but may introduce spurious oscillations at sharp discontinuities due to the Gibbs' phenomenon.

Table 1: Flow parameters for transonic turbine stage

Stator inflow angle, deg	0.0
Stator outflow angle, deg	73.5
Rotor-relative inflow angle, deg	56.5
Rotor-relative outflow angle, deg	−67.5
Stator inflow Mach number	0.14
Stator outflow Mach number	1.12
Rotor-relative inflow Mach number	0.58
Rotor-relative outflow Mach number	1.11
Rotor Mach number	0.60
Ratio of specific heats γ	1.27

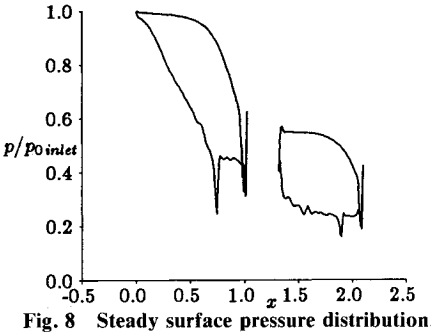

Fig. 8 Steady surface pressure distribution.

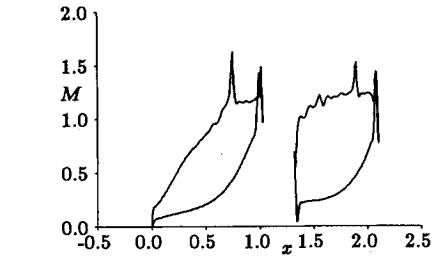

Fig. 9 Steady surface Mach number distribution.

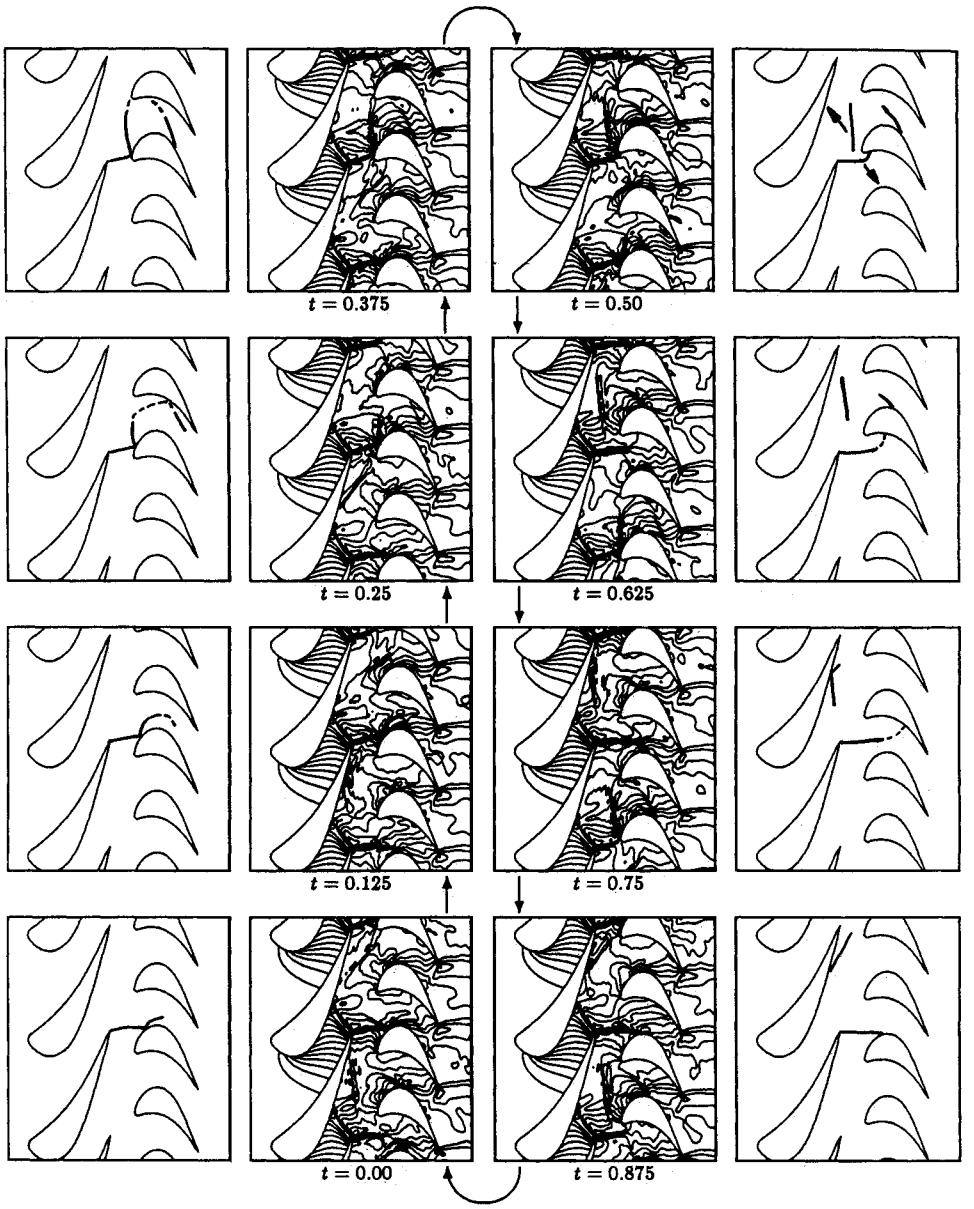

Fig. 10 Pressure contours in unsteady stator/rotor interaction.

To understand the motion of the shocks in the unsteady interaction, it is useful to note that the velocity of a very weak shock is a sum of the convection velocity of the local fluid plus a velocity of magnitude c, the speed of sound, normal to the shock. Thus, a stationary shock is actually one in which the combined vector propagates tangentially along the shock front such that the motion is not visible when the shock extends to infinity downstream.

Examining the pressure contours at the beginning of the period at $t = 0$ in the center of the figure, the oblique shock extending downstream from the trailing edge of the stator has hit the crown of the rotor suction surface, and a weak reflection is already visible. At $t = 0.125$, the reflection is growing much stronger, and the point of reflection has moved forward towards the leading edge as the rotor blade moves upward.

At $t = 0.25$, the reflected wave is still growing. In addition, the portion of the reflected wave that moved towards the pressure surface of the adjacent rotor has now reflected a second time and is moving back towards the original rotor. The pressure contours do not show this very clearly, but it is clear in a gray-scale animated videotape, which was produced to aid in the interpretation and understanding of the results, and it is indicated in Fig. 10. At $t = 0.375$, the primary reflection point has almost reached to the rotor leading edge. The secondary reflected wave has crossed back to the original rotor and intensified sufficiently so that it is again clearly visible in the pressure contours.

At $t = 0.50$, the primary reflection point has just passed the rotor leading edge. The reflected wave has left the rotor and is propagating upstream towards the stator suction surface. As discussed earlier, the propagation velocity is the sum of the local convection velocity and a velocity of magnitude c normal to the shock. This velocity is indicated in Fig. 10. Meanwhile, the secondary reflected shock has strengthened further and moved upstream. Actually the shock line appears to have moved upstream, but at each point on the shock, the motion is primarily normal to the flowfield since the flow on the suction surface is supersonic and does not permit disturbances to move upstream. The upstream motion is thus achieved by the pressure wave moving upstream through the subsonic flow near the pressure surface of the adjacent rotor and then moving across the flow to the original rotor. It appears to be, when the pressure wave moves into the higher Mach number flow, that it strengthens into a discernible shock.

At $t = 0.625$, the primary oblique shock has left the rotor. The dynamics can be understood by using the simplified shock motion theory given earlier. To a good approximation, the straight part of the oblique shock is a stationary shock in the

Fig. 11 Schlieren photograph of cascade flow with passing bars.

stator frame of reference, and therefore it propagates along its length with speed $\sqrt{u^2-c^2}$. This velocity is sufficiently great so that the straight portion will increase in length until (by coincidence) it reaches the rotor crown just as it hits it at time $t=0.875$. The curved diffracting part of the shock is weak and is continuing to weaken rapidly. The primary reflected shock is still propagating towards the upstream stator, and the secondary shock is still moving upstream.

At $t=0.75$, the primary oblique shock has almost regained its maximum length. The primary reflected shock has just struck the trailing edge of the upstream stator, and the secondary reflected shock has almost disappeared. Finally, at $t=0.875$, the primary oblique shock strikes the next rotor blade to begin the cycle again. The primary reflected shock is reflecting once more from the stator suction surface. This reflection is clearly visible at $t=0.0$ (which by periodicity corresponds to $t=1$), is barely visible at $t=0.125$, and disappears at $t=0.25$ when it strikes the rotor near the leading edge.

Figure 11 shows part of a schlieren photograph taken at Oxford University.[14,16] In the experiment, the rotors were stationary, and the stators were simulated by moving bars. These bars produce both shocks and wakes but do not model the secondary reflections off the suction surface. The shock reflection on the lower blade in Fig. 11 is comparable to the shock reflection on the lower rotor in Fig. 10 at $t=0.375$. Comparison with a number of other Schlierens shows the agreement in the shock motion is very good.

Consequences

The shocks striking the leading portion of the rotor suction surface will have a strong effect on the boundary layer. It has been observed experimentally that the primary shock reflection causes a temporary boundary-layer separation.[16] The separation bubble is convected downstream and then collapses into highly turbulent flow, which greatly increases the heat transfer and viscous losses. Also, Johnson[14] has shown that the pressure transients due to the unsteady shock reflections produce corresponding transients in the heat transfer due to the adiabatic compression of the boundary layer.

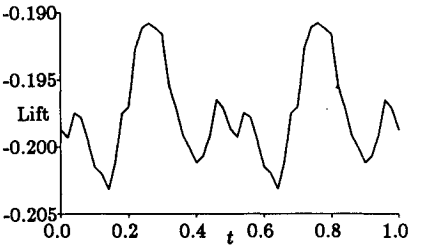

Fig. 12 Unsteady stator lift.

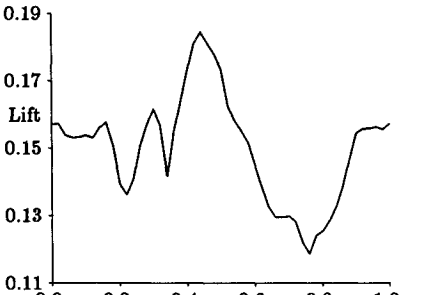

Fig. 13 Unsteady rotor lift.

Figures 12 and 13 show the unsteady lift on the stator and rotor. The lift is nondimensionalized using the stagnation inlet density and speed of sound and the stator chord. Because the calculation is performed with two stators and one rotor, Fig. 12 covers two periods with the time t being nondimensionalized with respect to twice the stator blade-passing period. There is a 6% peak-peak variation in lift despite the fact that the pressure is steady on all but a small portion of the stator suction surface near the trailing edge.

In Fig. 13, the time t has been nondimensionalized by the rotor blade-passing period. Under the influence of the strongly unsteady shock motion described earlier, there is a 40% peak-peak variation in lift. Also, because of the discontinuous nature of the shocks, there are abrupt changes in the lift. Thus, a Fourier decomposition of this lift would reveal structural excitation of the rotor blade at a large number of harmonics.

There are a number of possible consequences of the highly unsteady rotor lift. The large amplitude of the structural forcing at the lowest harmonic could produce significant blade oscillations, possibly leading to fatigue. The full spectrum of the structural excitation raises the possibility that one of the higher harmonics may be close to a natural frequency of the structure and may therefore produce an exceptionally large response. Also, one of the higher harmonics will be close to the frequency of the vortex shedding at the blunt trailing edge and so may excite and amplify this leading to increased base losses. The final consequence is that, associated with the unsteady lift, there must be an unsteady vortex sheet shed at the trailing edge. The kinetic energy of the unsteady part of the outflow, due to this vortex sheet, will eventually be dissipated, and so this represents an additional loss mechanism. The loss is proportional to the square of the vortex sheet strength, and hence the square of the unsteady lift. At low levels of unsteadiness, such as a 5% variation in lift, this loss will be negligible compared to other losses. However, at the 40% peak-peak level experienced by the rotor, this new loss mechanism may become significant.

Conclusions

This paper has presented a numerical method that is capable of predicting the strongly unsteady flow in a transonic stator/rotor interaction. A particular feature is the use of time-inclined computational planes to handle the difficulties posed by a stator/rotor pitch ratio, that is not a simple integer ratio. The conservative numerical method and the simple, conservative treatment of the interface between the stator and rotor

grids allow the accurate calculation of the stationary and moving shocks produced in the interaction. The unsteady shocks cause a 40% variation in the lift on the rotor. In addition to producing structural vibrations, it is conjectured that this high level of unsteadiness can lead directly to increased losses due to the shedding of an unsteady vortex sheet.

Acknowledgments

The author is grateful to M. L. G. Oldfield and A. B. Johnson for discussions on the comparison of the calculation with their Schlieren photographs and for supplying the photograph for Fig. 11. The author is also grateful to Rolls-Royce PLC for their financial support and P. Stow and A. Suddhoo for their technical support in the development of the computational method.

References

[1]Hodson, H. P., "An Inviscid Blade-to-Blade Prediction of a Wake-Generated Unsteady Flow," American Society of Mechanical Engineers, New York, ASME Paper 84-GT-43, June 1984.

[2]Giles, M. B., "Calculation of Unsteady Wake Rotor Interaction," *Journal of Propulsion and Power,* Vol. 4, No. 4, 1988, pp. 356-362.

[3]Koya, M., and Kotake, S., "Numerical Analysis of Fully Three-Dimensional Periodic Flows Through a Turbine Stage," *Journal of Engineering for Gas Turbines and Power*, Vol. 107, Oct. 1985, pp. 945-952.

[4]Fourmaux, A., "Unsteady Flow Calculation in Cascades," American Society of Mechanical Engineers, New York, ASME Paper 86-GT-178, 1986.

[5]Lewis, J. P., Delaney, R. A., and Hall, E. J., "Numerical Prediction of Turbine Vane-Blade Interaction," AIAA Paper 87-2149, June 1987.

[6]Rai, M. M., "Navier-Stokes Simulations of Rotor-Stator Interaction Using Patched and Overlaid Grids," AIAA Paper 85-1519, July 1985.

[7]Rai, M. M., "Unsteady Three-Dimensional Navier-Stokes Simulations of Turbine Rotor-Stator Interaction," AIAA Paper 87-2058, June 1987.

[8]Erdos, J. I., Alzner, E., and McNally, W. "Numerical Solution of Periodic Transonic Flow Through a Fan Stage," *AIAA Journal,* Vol. 15, No. 11, 1977, pp. 1559-1568.

[9]Ni, R.-H., "A Multiple Grid Scheme for Solving the Euler Equations," *AIAA Journal,* Vol. 20, No. 11, 1981, pp. 1565-1571.

[10]Giles, M. B., "UNSFLO: A Numerical Method for Unsteady Flow in Turbomachinery," MIT Gas Turbine Laboratory, Cambridge, MA, TR 195, 1988.

[11]Giles, M. B., "Generalized Conservation Cells for Finite Volume Calculations," AIAA Paper 87-1118, June 1987.

[12]Guenette, G. R., Epstein, A. H., Giles, M. B., Haimes, R., Norton, R. J. G., "Fully Scaled Transonic Turbine Rotor Heat Transfer Measurements," *Journal of Turbomachinery,* Vol. 111, Jan. 1989, pp. 1-7.

[13]Ashworth, D. A., LaGraff, J. E., Schultz, D. L., Grindrod, K. J., "Unsteady Aerodynamic and Heat Transfer Processes in a Transonic Turbine Stage," *Journal of Engineering for Gas Turbines and Power*, Vol. 107, Oct. 1985, pp. 1022-1030.

[14]Johnson, A. B., Rigby, M. J., Oldfield, M. L. G., Ainsworth, R. W., and Oliver, M. J., "Surface Heat Transfer Fluctuations on a Turbine Rotor Blade due to Upstream Shock Wave Passing," *Journal of Turbomachinery,* Vol. 111, April 1989, pp. 105-115.

[15]Giles, M. B., "Developments in the Calculation of Unsteady Turbomachinery Flow," Numerical Methods for Fluid Dynamics III, edited by K. W., Morton and M. J. Baines, Oxford Univ. Press, Oxford, England, UK, 1988 pp. 45-64.

[16]Schultz, D. L., Ashworth, D. A., LaGraff, J. E., Rigby, M. J., Johnson, A. B., "Wake and Shock Interactions in a Transonic Turbine Stage," AGARD PEP CP-401, 1986.